Hindawi
International Journal of Antennas and Propagation
Volume 2022, Article ID 9982602, 7 pages
https://doi.org/10.1155/2022/9982602

*Research Article*

# Broadband Compact MIMO Antenna Employing CRLH Transmission Lines with High Isolation

**Liangyuan Liu and Xiangqun Shi**

*Zhongshan Institute, University of Electronic Science and Technology of China, Zhongshan, China*

Correspondence should be addressed to Liangyuan Liu; liuly1997@126.com

Received 6 May 2022; Accepted 29 July 2022; Published 27 August 2022

Academic Editor: Chien-Jen Wang



A broadband and planar multiple-input multiple-output (MIMO) antenna with pattern diversity is presented in this letter. The four-port MIMO antenna is designed by using a novel metamaterial structure with small dimensions of $60 \times 60 \times 1.6\,\text{mm}^3$. Each radiating element of the MIMO antenna is comprised of composite right/left-hand (CRLH) transmission lines (TLs). Between its four elements, there are four open L-shaped slot loading on the ground plane of the patch antenna system. The antenna obtains the wide frequency range of 2.31–4.99 GHz. In addition, The proposed antenna has an isolation greater than 20 dB between its four elements. The MIMO antenna has excellent bandwidth performance and good diversity properties between elements.

## 1. Introduction

Design of MIMO antennas encounters many challenges, such as miniaturization and high isolation. Unlike the traditional MIMO antennas, the metamaterial MIMO antennas have many advantages of electrically small size, high isolation, low profile, and broadband width. The development of high speed, high capacity, energy saving, and emission reduction in the global mobile communication network has led to the characteristics of miniaturization, broadband, and integration on the development trend of mobile communication antenna. By multiple antennas, the multiple-input multiple-output (MIMO) technology is used to suppress multipath channel fading, improve system capacity, and reduce channel error rate. To set up multiple antennas on platforms with limited mobile terminals, it requires miniaturization of antennas and small cell spacing. The research of comb-line inductor, complementary open resonant ring and slot capacitor provides new ideas for miniaturization, high isolation, wide bandwidth, and low mutual coupling of MIMO antenna elements. The high isolation of 5G smart phone antenna unit is realized by a comb-line structure.

Metamaterials with negative permeability and permittivity can be used to design subwavelength cavity resonators, which miniaturizes the antenna [1]. Itoh reports the basic principles of compound left/right-handed (CRLH) transmission lines. The broadband and miniaturization of antenna unit is realized by CRLH transmission line structure with tunable radiation angle [2]. A MIMO antenna using slotted-complementary split-ring resonators can minimize mutual coupling between two coplanar microstrip antennas [3]. A planar compact metamaterial-substrate antenna array based on the resonator structures is presented [4]. The monopole antenna loading on metamaterial can effectively control electromagnetic wave propagation [5]. A compact wideband MIMO antenna loaded a split-ring resonator (SRR) with the orthogonal arrangement, having a good isolation and low correlation diversity performance between elements, is presented [6]. Based on the theory of characteristic modes (TCM), a planar UWB mobile MIMO antenna is able to excite different modes, which realize the desired diverse radiation patterns and high isolation [7]. The mushroom body metamaterial dielectric structure is used to reduce the space size of base station antenna and isolation can be improved by introducing planar-modified mushroom structures [8]. The electromagnetic bandgap structures and metasurfaces can enhance the isolation [9, 10]. A four-element MIMO antenna system loading complementary split-

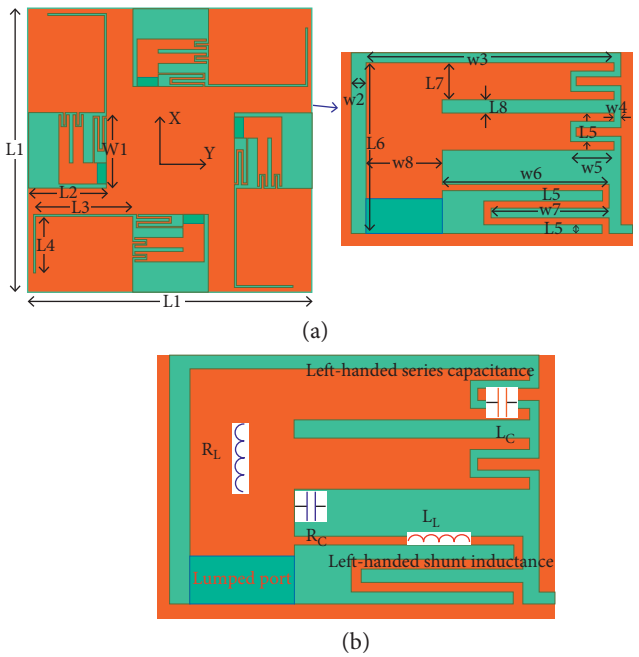


Figure 1: (a) Configuration parameters of the four-port antenna. (b) Configuration with corresponding lumped elements.

Table 1: Optimal physical dimensions of the MIMO antenna.

| Parameters | L1 | L2 | L3 | L4 | L5 | L6 | L7 | L8 |
|---|---|---|---|---|---|---|---|---|
| Dimensions | 60 | 16 | 21 | 12 | 0.5 | 10.5 | 2.5 | 1.4 |
| Parameters | W1 | W2 | W3 | W4 | W5 | W6 | W7 | W8 |
| Dimensions | 16 | 1 | 14.5 | 0.5 | 2.6 | 9.5 | 7 | 4.5 |

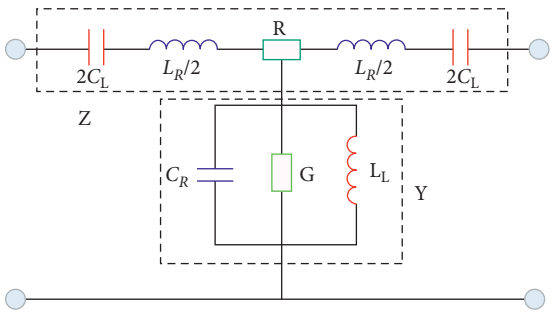


Figure 2: Equivalent circuit diagram of the CRLH TLs.

ring resonator (CSRR) on its ground plane has highly compact patch elements [11]. The parasitic elements are introduced to reduce mutual coupling [12, 13]. The defected ground structures (DGS) with the opposite original characteristic modes currents blocks the coupling modes, thus reducing mutual coupling and improving port isolation [14]. However, this antenna requires a large overall antenna size and the antenna gain is approximate 0 dB. By self-cancellation of the near-field currents and induced ground, the mutual coupling of two close metamaterial-inspired antennas is reduced [15]. A pattern-diversity-based method is proposed to reduce mutual coupling [16, 17]. DGS can be introduced to 5G MIMO antenna [18, 19].

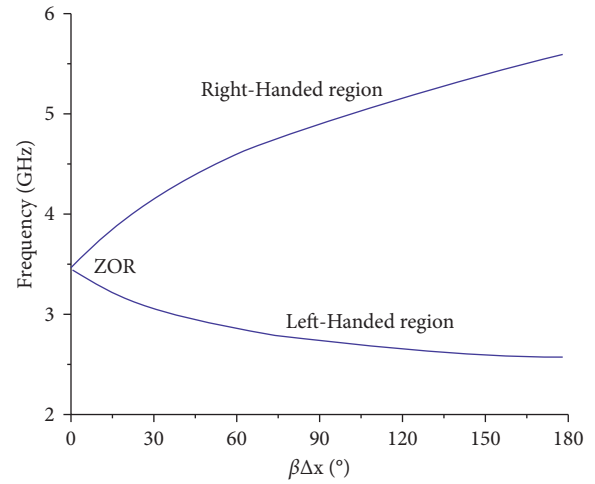


Figure 3: Dispersion diagram characteristic of the proposed CRLH-TL antenna.

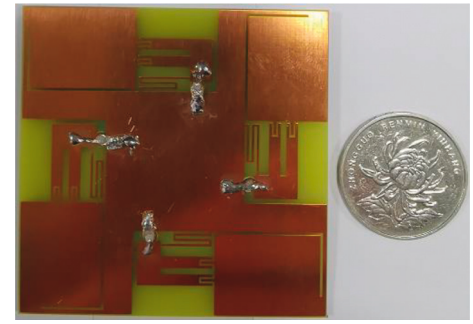

Figure 4: Photograph of the fabricated MIMO antenna.

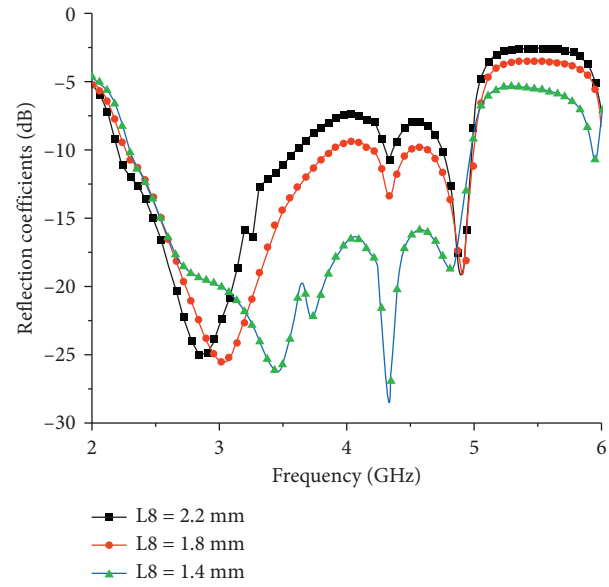


Figure 5: Simulated reflection coefficients of the MIMO antenna for different widths of the printed width L8.

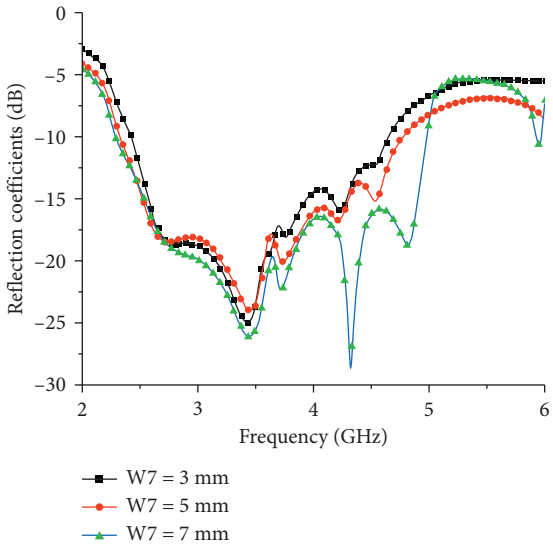


Figure 6: Simulated reflection coefficients of the proposed MIMO antenna with the varied width W7.

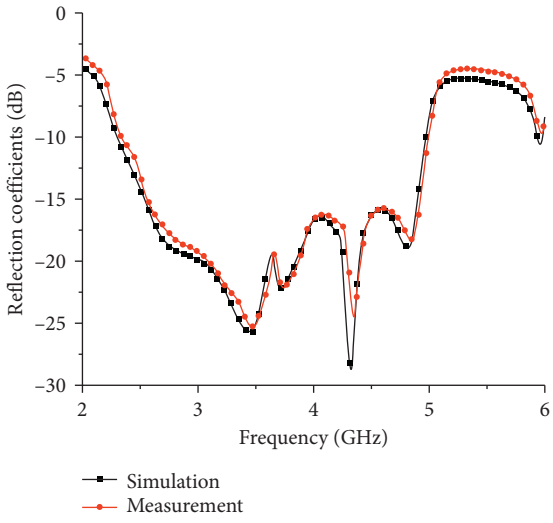


Figure 7: Simulated and measured reflection coefficients of the proposed antenna.

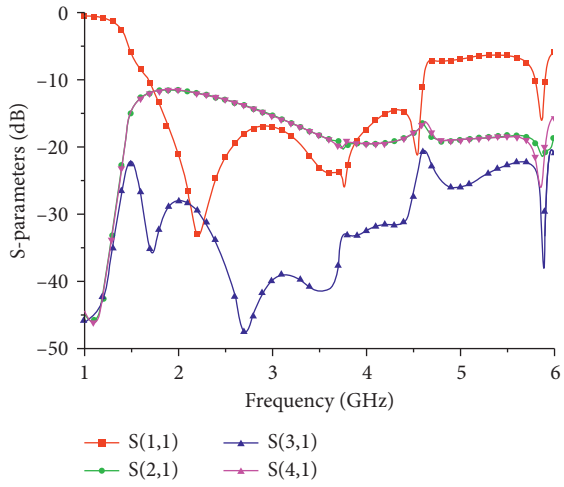


Figure 8: The simulated isolation performance of the MIMO antenna without slot.

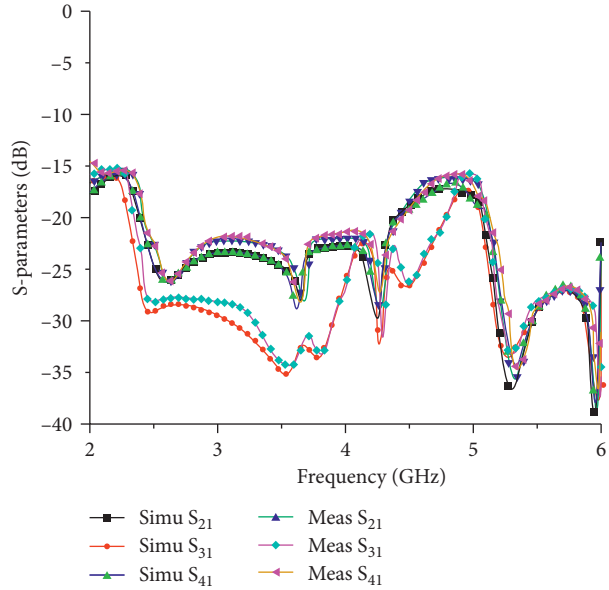


Figure 9: The simulated and measured isolation performance of the MIMO antenna with DGS.

Based on the CRLH-TL concept, the metamaterial MIMO antenna of this project has a smaller space size, wider bandwidth, smaller coupling between units, which can support high data transmission rate, high frequency spectrum utilization, and greater flexibility. Unlike the existing mobile terminal antenna mentioned above, the ground and inverted-F patch form a CRLH-TLs resonance. It should be pointed out that the pattern diversity method can excite different characteristic modes to obtain better isolation. A metal patch embedded with two interdigital capacitors acts as the main radiator. A small comb strip is placed between the microstrip line and ground. Four same antenna elements are placed on the orthogonal edges of a rectangular ground plane to meet the MIMO communication needs. The experimental results show that performance of the proposed antenna can work well for the mobile MIMO antenna. The bandwidth of the antenna is 2.68 GHz (2.31–4.99 GHz), which is a suitable candidate for Bluetooth, WLAN, WiMAX, 5G communication application, and satellite communications.

## 2. Antenna Design

The structure of the mobile MIMO antenna is shown in Figure 1. The MIMO antenna is composed of three parts: four inverted-F radiation elements, four feed ports, and a coplanar ground plane. The antenna is printed on the FR4 substrate with a dielectric constant of 4.4, a thickness of 1.6 mm, and a loss tangent of 0.025. The thickness of covered copper layers is 35 um. A set of interdigital gap is etched on between the host inverted-F patch and the coplanar ground, which forms left-handed series capacitance. The left-handed shunt inductance is resulted from the small comb strip. The

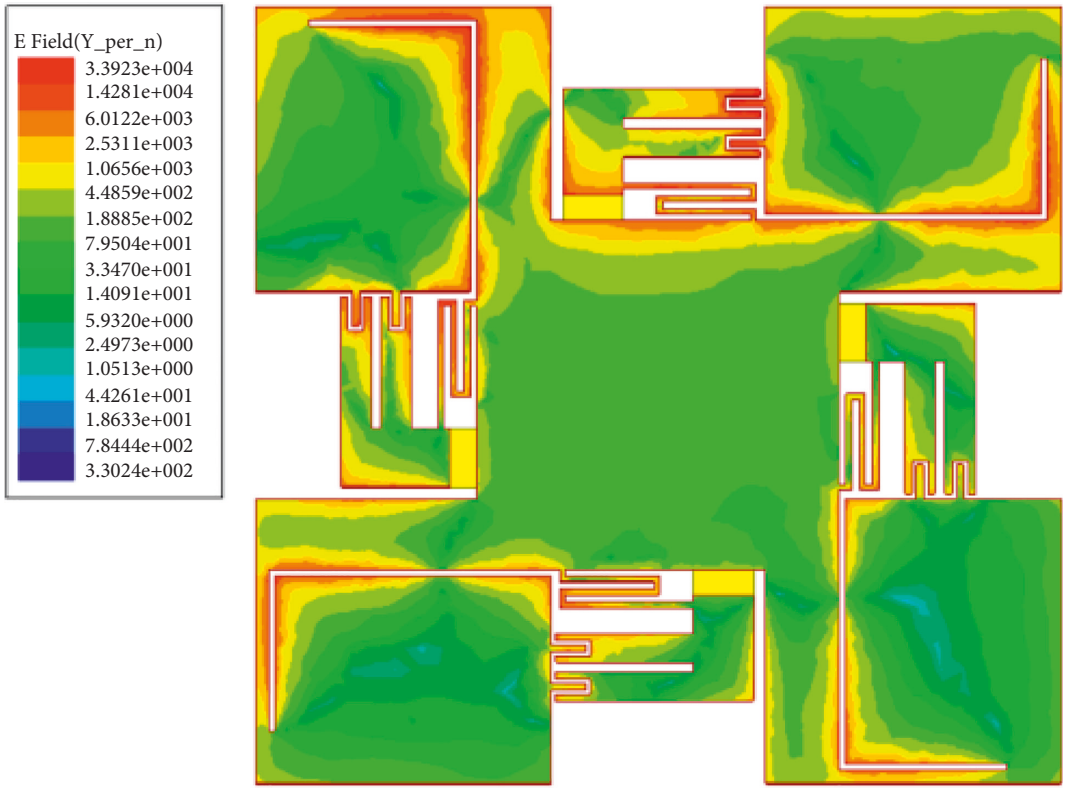


Figure 10: The simulated electric field intensity of the MIMO antenna in 3.63 GHz.

left-handed series capacitance and the left-handed shunt inductance can provide a via-free left-handed transmission line, which can excite the backward radiating wave. At the same time, the series inductance $L_R$ is formed from the current flow on the inverted-F patch. The shunt capacitance $C_R$ results from the electric field between the inverted-F patch and coplanar ground. The series inductance and the shunt capacitance compose a right-handed transmission line which can induce a forward radiating wave.

The physical dimensions of optimized parameters are summarized in Table 1.

An equivalent circuit model for the via-free CRLH is shown in Figure 2. A small comb strip is placed between the feed point and the coplanar ground plane. The inverted-F patch and the coplanar ground form a CRLH-TLs resonant cavity. Because the phase of backward wave is complementary, the zeroth-order resonance (ZOR) is inspired. The size of four element antenna is effectively decreased, which can realize a subwavelength resonant cavity.

According to the Bloch-Floquet theorem and the equivalent circuit diagram of the CRLH-TLs resonant cavity [1], the dispersion relation can be calculated as follows:

$$\cos(\beta\Delta x) = 1 + \frac{1}{2}\left(j\omega L_R + \frac{1}{j\omega C_L}\right)\left(j\omega C_R + \frac{1}{j\omega L_L}\right). \quad (1)$$

The CRLH-TLs subwavelength resonance has many resonant frequencies with the phase constant of electromagnetic waves $\beta = 0$. An subwavelength resonance occurs when

$$\beta_n = n\frac{\pi}{l}n = 0, \pm 1, \ldots, \pm (N-1), \quad (2)$$

where $n$ is the mode numbers and $l$ is the electrical length of the CRLH-TLs resonator. Because of the novel CRLH-TL subwavelength resonance, the antenna effective length has been greatly reduced. The antenna bandwidth has been broadened simultaneously.

The S-parameter simulation and measurement are convenient, and the transfer matrix is easy to be converted into parameters. It is easy to judge the characteristics of the transfer matrix by using the S-parameter simulation and measured values. The dispersion diagram of the CRLH TL is obtained using (3).

$$\cos(\beta\Delta x) = \frac{1 - S_{11}S_{22} + S_{12}S_{21}}{2S_{21}}. \quad (3)$$

The dispersion diagram of the CRLH-TL antenna is plotted in Figure 3. The ZOR occurs at 3.46 GHz, where the value of $\beta\Delta x = 0$. When the frequency is low, it shows left-handed characteristics. The phase velocity in the transmission line is negative and there is backward wave transmission. When the frequency is high, it shows the right-hand characteristics. The phase velocity in the transmission line is positive and there is forward wave transmission. Owing to infinite wavelength of the ZOR frequency, the design and fabrication dimensions are particularly compact.

The fabricated MIMO antenna is shown in Figure 4. Four SMA connectors are used to feed to the antenna from the bottom.

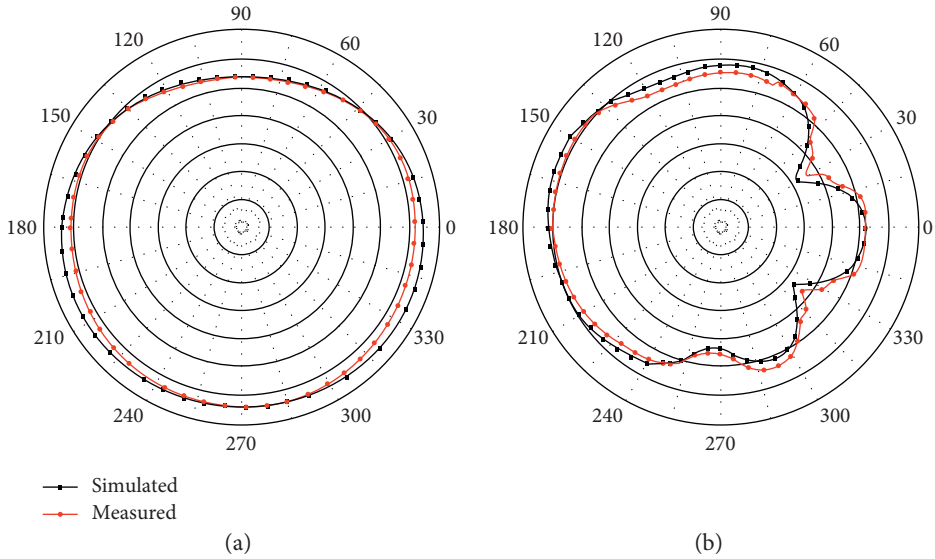


FIGURE 11: Measured gain for the 4-element MIMO antenna. (a) x-z plane and (b) x-y plane.

## 3. Simulation and Experimental Results

To verify the simulations and optimizations, the planar MIMO antenna has been performed using HFSS16 Microwave Studio simulation tool. The effects of the -10 dB impedance bandwidth are presented in Figures 5 and 6.

The effects of different width L8 parameters on the impedance bandwidth of the MIMO antenna are illustrated in Figure 5. As shown in figure 5, the resonance frequencies shift ward with the decrease of L8. With the decrease of L8, the bandwidth becomes wider and the resonance of the intermediate frequency part becomes deeper.

It is observed in Figure 6 that the resonance frequencies shift downward with the increase of W7. With the increase of W7, the bandwidth becomes wider. The impedance matching becomes good and the bandwidth is gradually widen.

The S parameters of the four-port MIMO antenna is measured by using a network analyzer Agilent E8361 A as shown in Figure 7. The simulated −10 dB bandwidth is 2.69 GHz (2.28–4.97 GHz). The measured −10 dB bandwidth is 2.68 GHz (2.31–4.99 GHz). The fractional bandwidth for the four ports is as much as 73.8%. The simulated and measured results agree well.

S parameters $S_{21}$, $S_{31}$, and $S_{41}$ of the MIMO antennas are presented in Figure 8, respectively. Because of the symmetrical structure, $S_{21}$ and $S_{41}$ are almost identical. The isolation without decoupled structure is relatively low.

To improve the isolation, the defected ground structures (DGS) are introduced to block the coupling modes at certain locations. DGS can significantly affect the surface current of the chassis and the noncoupling modes. Figure 9 shows the simulated and measured isolation performance of the MIMO antenna with DGS. As can be seen from figure 9, the measured values of $S_{21}$, $S_{31}$, and $S_{41}$ are basically consistent with the simulated values. Compared with $S_{21}$ and $S_{41}$, $S_{31}$ is smaller due to the long distance. As can be seen from figure 9, the MIMO antenna with decoupling structure has a small value of $S_{21}$, $S_{31}$, and $S_{41}$. It is already obvious that the all $S_{21}$, $S_{31}$, and $S_{41}$ values are less than −20 dB at entire operating impedance bandwidth. In the entire operating band, the MIMO antenna has a low envelope co-relation coefficient (ECC<0.003), a high diversity gain (DG > 9.999).

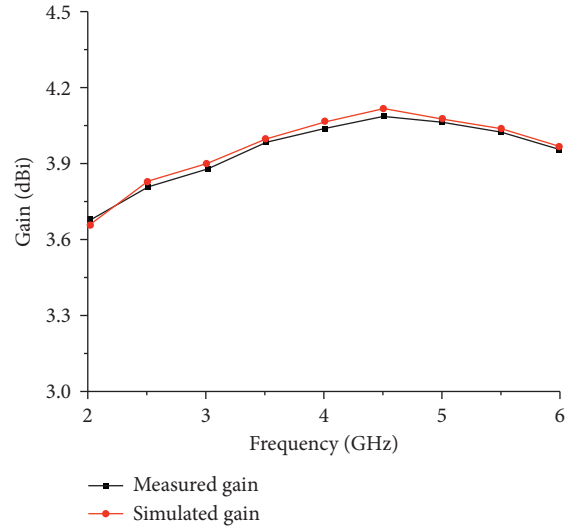


FIGURE 12: Measured radiation gain of the proposed antenna in the +Z direction.

The simulated electric field intensity in 3.63 GHz is analyzed in Figure 10. The electric field around the ground gap is stronger. The defected ground structures improve antenna isolation.

The normalized measured gain patterns for the 4-element MIMO antenna at 3500 MHz are shown in Figure 11. The measured highest gain is 4.25 dBi. Figure 12 shows the measured and simulated radiation gain of the CRLH-TLs MIMO antenna. The total radiation efficiencies are above 75%. The peak efficiency is 90% at 3.8 GHz.

Table 2: Performance comparison with previous antennas.

| | Antenna size (mm ∗ mm) | Total size | Bandwidth (GHz) | Isolation (dB) | Gain (dBi) |
|---|---|---|---|---|---|
| Reference [12] | $100 \times 112$ | $0.63\lambda_0 \times 0.71\lambda_0$ | 1.87–1.94 | 20 | 4.2 |
| Reference [13] | $66 \times 72$ | $0.78\lambda_0 \times 0.85\lambda_0$ | 2.25–2.63,3.4–3.7,5.12–5.39 | 14 | 3.99 |
| Reference [16] | $70 \times 140$ | $0.63\lambda_0 \times 1.26\lambda_0$ | 2.6–2.8,3.4–3.6 | 20 | 3.9 |
| Reference [17] | $40 \times 100$ | $0.47\lambda_0 \times 1.17\lambda_0$ | 3.5–3.6 | 15 | 4.15 |
| This work | $60 \times 60$ | $0.62\lambda_0 \times 0.62\lambda_0$ | 2.31–4.99 | 20 | 4.25 |

The proposed MIMO technique is compared with some previously presented antennas as shown in Table 2.

where $\lambda_0$ is the free space wavelength at the center resonant frequency.

## 4. Conclusions

In this letter, a novel broadband metamaterial MIMO antenna has been presented. Miniaturization and broadband are finally accomplished by introducing an organic integration of metamaterials, orthogonal structure, and separated four-directional L-shaped slot decoupling. The simulation and measurement results confirm that the MIMO antenna has excellent bandwidth performance. Both the simulated and measured results of S parameters demonstrate that the four-port MIMO antenna could offer an higher isolation of better than 20.0 dB in the operating range. With an overall dimension of $60 \times 60 \times 1.6\,\text{mm}^3$, the bandwidth of the antenna is 2.68 GHz (2.31–4.99 GHz). The proposed MIMO antenna is a potential candidate in portable wireless routers for a 5G communication system. A metal inverted-F patch embedded with a set of interdigital gap acts as the main radiation element.

## Data Availability

The data used to support the findings of this study are included within the article.

## Conflicts of Interest

The authors declare that they have no conflicts of interest regarding this article.

## Acknowledgments

This work was supported in part by Educational Commission of Guangdong Province (Grant nos. 26-420N14 and SZY202002) and Science and Technology Project of Zhongshan city (Grant nos. 26-419S45, Zhongshan Institute of UESTC (Grant no. 26-417YKQ19).

## References

[1] N. Engheta, "An idea for thin subwavelength cavity resonators using metamaterials with negative permittivity and permeability," *IEEE Antennas and Wireless Propagation Letters*, vol. 1, pp. 10–13, 2002.

[2] S. Lim, C. Caloz, and T. Itoh, "Metamaterial-based electronically controlled transmission-line structure as a novel leaky-wave antenna with tunable radiation angle and beamwidth," *IEEE Transactions on Microwave Theory and Techniques*, vol. 52, no. 12, pp. 2678–2690, 2004.

[3] M. M. Bait-Suwailam, O. F. Siddiqui, and O. M. Ramahi, "Mutual coupling reduction between microstrip patch antennas using slotted-complementary split-ring resonators," *IEEE Antennas and Wireless Propagation Letters*, vol. 9, pp. 876–878, 2010.

[4] P. Mookiah and K. R. Dandekar, "Metamaterial-substrate antenna array for MIMO communication system," *IEEE Transactions on Antennas and Propagation*, vol. 57, no. 10, pp. 3283–3292, 2009.

[5] D. A. Ketzaki and T. V. Yioultsis, "Metamaterial-based design of planar compact MIMO monopoles," *IEEE Transactions on Antennas and Propagation*, vol. 61, no. 5, pp. 2758–2766, 2013.

[6] R. Anitha, P. V. Vinesh, K. C. Prakash, P. Mohanan, and K. Vasudevan, "A compact quad element slotted ground wideband antenna for MIMO applications," *IEEE Transactions on Antennas and Propagation*, vol. 64, no. 10, pp. 4550–4553, 2016.

[7] X. Zhao, S. P. Yeo, and L. C. Ong, "Planar UWB MIMO antenna with pattern diversity and isolation improvement for mobile platform based on the theory of characteristic modes," *IEEE Transactions on Antennas and Propagation*, vol. 66, no. 1, pp. 420–425, 2018.

[8] S. Kahng, J. Jeon, J. Anguera, and T. Park, "A compact MIMO antenna using CRLH configuration double-layered folded ring radiations with planar mushroom decoupling structure," *IEEE Antennas and Propagation Magazine*, vol. 57, no. 2, pp. 123–130, 2015.

[9] G. Zhai, Z. N. Chen, and X. Qing, "Enhanced isolation of a closely spaced four-element mimo antenna system using metamaterial mushroom," *IEEE Transactions on Antennas and Propagation*, vol. 63, no. 8, pp. 3362–3370, 2015.

[10] C. C. Hsu, K. H. Lin, and H. L. Su, "Implementation of broadband isolator using metamaterial-inspired resonators and a T-shaped branch for MIMO antennas," *IEEE Transactions on Antennas and Propagation*, vol. 59, no. 10, pp. 3936–3939, 2011.

[11] M. S. Sharawi, M. U. Khan, A. B. Numan, and D. N. Aloi, "A CSRR loaded MIMO antenna system for ISM band operation," *IEEE Transactions on Antennas and Propagation*, vol. 61, no. 8, pp. 4265–4274, 2013.

[12] Z. Li, Z. Du, M. Takahashi, K. Saito, and K. Ito, "Reducing mutual coupling of MIMO antennas with parasitic elements for mobile terminals," *IEEE Transactions on Antennas and Propagation*, vol. 60, no. 2, pp. 473–481, 2012.

[13] G. H. Li, H. Q. Zhai, Z. H. Ma, C. H. Liang, R. D. Yu, and S. Liu, "Isolation-improved dual-band MIMO antenna array for LTE/WiMAX mobile terminals," *IEEE Antennas and Wireless Propagation Letters*, vol. 13, pp. 1128–1131, 2014.

[14] A. Ghalib and M. S. Sharawi, "TCM analysis of defected ground structures for MIMO antenna designs in mobile terminals," *IEEE Access*, vol. 5, pp. 19680–19692, 2017.

[15] J. Zhu and G. V. Eleftheriades, "A simple approach for reducing mutual coupling in two closely spaced metamaterial-

inspired monopole antennas," *IEEE Antennas and Wireless Propagation Letters*, vol. 9, pp. 379–382, 2010.

[16] R. Karimian, H. Oraizi, S. Fakhte, and M. Farahani, "Novel F-shaped quad-band printed slot antenna for WLAN and WiMAX MIMO systems," *IEEE Antennas and Wireless Propagation Letters*, vol. 12, pp. 405–408, 2013.

[17] C. F. Ding, X. Y. Zhang, C. D. Xue, and C. Y. D. Sim, "Novel pattern-diversity-based decoupling method and its application to multielement MIMO antenna," *IEEE Transactions on Antennas and Propagation*, vol. 66, no. 10, pp. 4976–4985, 2018.

[18] Y. U. Devi, M. T. Boddapati, T. A. Kumar, C. K. Kavya, and P. Pardhasaradhi, "Conformal printed MIMO antenna with DGS for millimetre wave communication applications," *International Journal of Electronics Letters*, vol. 8, no. 3, pp. 329–343, 2020.

[19] M. V. Rao, B. T. P. Madhav, J. Krishna, Y. U. Devi, T. Anilkumar, and B. P. Nadh, "CSRR-loaded T-shaped MIMO antenna for 5G cellular networks and vehicular communications," *International Journal of RF and Microwave Computer-Aided Engineering*, vol. 29, pp. 1–14, 2019.